Journal of Bone and Mineral Metabolism (2019) 37:455–466
https://doi.org/10.1007/s00774-018-0953-9

ORIGINAL ARTICLE

Umbilical cord mesenchymal stem cell conditioned medium restored the expression of collagen II and aggrecan in nucleus pulposus mesenchymal stem cells exposed to high glucose

Lei Qi[1] · Ran Wang[2] · Qing Shi[2] · Ming Yuan[2] · Min Jin[2] · Dong Li[2,3]

Received: 15 June 2017 / Accepted: 21 August 2018 / Published online: 5 September 2018

Abstract

Diabetes can cause intervertebral disc degeneration by accelerating apoptosis and senescence of nucleus pulposus mesenchymal stem cells (NPMSCs). The aim of this study was to determine the effect of umbilical cord mesenchymal stem cells (UCMSCs) conditioned medium on high glucose (HG) induced degradation of NPMSCs produced extracellular matrix. NPMSCs were isolated from the inner intervertebral disc tissue using type XI collagenase digestion. According to Annexin V/propidium iodide (PI) flow cytometry analysis; HG leads to an increase in the rate of NPMSCs apoptosis. HG injury also resulted in a marked decrease in the percentage of cells in G0/G1 phase and an increase in cells in S and G2/M phases, indicating that HG induces cell cycle arrest of NPMSCs. Treatment with MSC-CM abolished the effect of HG on cell senescence. HG also significantly inhibited collagen II and aggrecan expression in NPMSCs. After MSC-CM treatment, the expression of these two extracellular matrix components was restored. Exposure to HG resulted in phosphorylation of p38 MAPK, while the levels of total p38 MAPK were not affected. When treated with MSC-CM, phosphorylated p38 MAPK levels of NPMSCs were lower than those without CM treatment. Our data also showed that p38 MAPK inhibitor SB203580 can attenuated phosphorylation of p38 MAPK and resumed the collagen II and aggrecan expression in NPMSCs. In summary, this study demonstrated that MSC-CM has the potential to alleviate HG induced extracellular matrix degradation via the p38 MAPK pathway.

Keywords Umbilical cord mesenchymal stem cells · Conditioned medium · Nucleus pulposus mesenchymal stem cells · Hyperglycemia · Extracellular matrix

Introduction

Intervertebral disc degeneration (IDD), a major cause of low back pain, is characterized by a progressive decrease of the proteoglycan content within the nucleus pulposus (NP). This results in disc dehydration and loss of its morpho-functional and biomechanical properties. The NP has been shown to be closely associated with chronic inflammation and diabetes mellitus, which can seriously affect patients' quality of life quality, particularly those in the elderly population [1, 2]. Diabetes can cause IDD by accelerating the apoptosis and senescence of NPMSCs. All forms of diabetes are characterized by hyperglycemia. Hyperglycemia is associated with ischemic injury that preferentially affects organs with non-redundant end capillary circulation [3, 4]. Accordingly, any injury to the capillary bed adjacent to the endplate could also contribute to disc degeneration by reducing the nutrient supply to the endplate and disc [5]. Besides reducing disc nutrient supply, diabetes can also lead to a reduction in disc glycosaminoglycan and water content, and these degenerative changes correlate with increased vertebral endplate thickness, decreased endplate porosity and with higher levels of the advanced glycation end-product (AGE), pentosidine [6, 7].

✉ Dong Li
lidong73@sdu.edu.cn

[1] Department of Orthopaedics, Qilu Hospital of Shandong University, Jinan 250012, Shandong, People's Republic of China

[2] Cryomedicine Laboratory, Qilu Hospital of Shandong University, Jinan 250012, Shandong, People's Republic of China

[3] Stem Cell and Regenerative Medicine Research Center of Shandong University, Jinan 250012, Shandong, People's Republic of China

Degeneration is characterized by increased degradation of the normal NP cell matrix by locally produced matrix metalloproteinases (MMPs) and a disintegrin and metalloproteinase with thrombospondin motifs (ADAMTS). In addition, the nature of the matrix produced in the degenerate NP differs from that in normal NPs, switching from type II collagen to type I collagen and changes in the synthesis of the proteoglycans from aggrecan to versican, biglycan, and decorin [1, 8]. Sixteen weeks after injecting streptozotocin (STZ), proteoglycan and collagen II levels in the extracellular matrix (ECM) of NPMSCs in a diabetic rat model were decreased compared with the control group. The resultant changes within the ECM have a number of consequences, resulting in loss of structural integrity, decreased hydration, and a reduced ability to withstand load [9].

In recent years, cell-based regenerative medicine, such as the use of mesenchymal stem cells (MSCs) or platelet-rich plasma (PRP), offer a promising approach to treat IDD. Hu et al. used bone marrow MSCs (BMMSCs) to inhibit interleukin-1 beta (IL-1β) induced degenerative effects in NPMSCs by a paracrine mechanism [10]. Cunha et al. assessed systemic transplantation of allogeneic BM-MSCs intravenously into a rat NP lesion model 24 h after injury, and achieved successful NP tissue regeneration [11]. Further studies suggest that cell therapies administered at an early stage of injury/disease onset may have greater chances of mitigating matrix loss, possibly through promotion of MSC activity by the inflammatory microenvironment associated with the injury itself [12]. Moreover, adipose mesenchymal stromal cell (ADSC) treatment resulted in a significant increase of aggrecan tissue levels in the degenerated disc, potentially being a new cell-based treatment of IDD [13]. In a clinical trial, chronic back pain patients treated with allogeneic BMMSCs displayed a quick and significant improvement in algofunctional indices versus controls [14]. Molecularly, researchers found that tromal cell-derived factor-1 (SDF-1)/CXC receptor 4 (CXCR4) signaling played a crucial role in MSC-based therapy for degenerated NPMSCs [15]. Yang et al. reported that BMMSC therapy promoted TGF-β1 expression in the NP, leading to anti-inflammatory effects via the inhibition of nuclear factor-kappa B (NF-κB), and the amelioration of disc degradation due to increased expression of collagen II and aggrecan in the degenerative intervertebral disc [16].

However, current research in stem cell-based therapy is mainly focused on inflammatory injury of the NP. The aim of this study was to determine the effect of MSCs on high glucose (HG) induced degradation of nucleus pulposus mesenchymal stem cells (NPMSCs) ECM and elucidate the possible mechanism of MSC conditioned medium (MSC-CM) to alleviate HG injury of NPMSCs. Previous studies have revealed that exosomes derived from hUCMSC plays a positive role in the repair of tissue damage [17], so we separated exosomes from MSC-CM (hUCMSC-EXO) and analyzed its microRNA (miRNA) components. Mitogen-activated protein kinase (MAPK) signaling pathway has also been demonstrated to be key mediators of IDD [18], and we also investigated whether MAPK pathway is implicated during MSC-CM treatment.

Materials and methods

Sample collection and ethical approval

Human umbilical cords were obtained from normal pregnancies in the Department of Obstetrics of Qilu Hospital. Intervertebral disc tissue samples were obtained from five males and four females aged 14–20 years (mean 16.2 years) who underwent deformity correction surgery for idiopathic scoliosis (IS) at Qilu hospital patients. These patients had no degenerative disc disease. The use of human umbilical cords and intervertebral disc samples was approved by the Ethics Committee of Shandong University, Qilu hospital, and written informed consent was obtained from all participants.

Culture of human umbilical cord mesenchymal stem cells (hUCMSCs) and preparation of conditioned medium

Culture of human umbilical cord mesenchymal stem cells (hUCMSC) was carried out in accordance with our published papers [19]. Briefly, hUCMSCs were cultured in Dulbecco's modified Eagle's medium (DMEM)/F-12 (Gibco; Thermo Fisher Scientific Inc., Waltham, MA, USA) supplemented with 10% fetal bovine serum (FBS; Gibco), 100 U/mL penicillin (Gibco) and 100 g/mL streptomycin (Gibco) in a fully humidified atmosphere with 5% CO_2 and 21% O_2 at 37 °C. The UCMSCs used throughout this study were between passages (P) 3 and 6. UCMSCs were deemed confluent when they reached 70–80% confluency and fresh full medium was replaced 24 h before harvesting. After 24 h, the medium was collected and centrifuged at 1000 g for 20 min with 0.1 μm pore filter to remove detached MSCs and cellular debris. This medium constituted the MSC-CM that NPMSCs would be subsequently treated with. MSC-CM was stored at − 80 °C until use.

hUCMSC-EXO microRNA array analysis

For exosome collection, MSC-CM was ultra centrifuged with 100,000*g* for 10 h at 4 °C. Two microgram aliquots of total RNA was isolated from hUCMSC-EXO using TRIzol reagent (Life Technologies). cDNAs were synthesized according to the manufacturer's protocol (Exiqon, Vedbaek, Denmark) and Enzyme mix (Exiqon). Array analyses

were performed using microRNA PCR arrays (SYBR Green master mix) (Exiqon) on an ABI PRISM7900 system (Applied Biosystems, Rockford, IL, USA); $n = 3$.

Isolation of NPMSCs

Intervertebral disc tissue was dissected into the inner and outer annulus fibrosus and the NP. The NP was then isolated for subsequent use. The NPMSCs were isolated by incubating the diced tissue overnight at 37 °C in 0.8 mg/mL type XI collagenase (Sigma-Aldrich) containing 1.67 U/mL DNase (Sigma-Aldrich). The tissue debris and cells obtained after digestion were centrifuged at 120 *g* for 10 min. The cell pellet was re-suspended and grown in DMEM/F-12 (Gibco) supplemented with 10% FBS in a fully humidified atmosphere with 5% CO_2 and 21% O_2 at 37°C. The cells were passaged twice before use.

Cell phenotyping of hUCMSCs and NPMSCs

Flow cytometry was performed to characterize UCMSCs and NPMSCs. The following cell surface epitopes were detected with anti-human CD24, CD29, CD45, CD73, CD90, and CD105 (BD Pharmingen, San Diego, CA, USA) compared with corresponding isotype control antibodies. 1×10^6 cells were stained with 10 µL of each specific fluorescence labeled antibodies in 100 µL of phosphate buffered saline (PBS) for 15 min at room temperature. Flow cytometry was performed with the Guava easyCyte 6HT (EMD Millipore, Billerica, MA, USA), and the data examined with Guava Incyte software (2.8 version, EMD Millipore).

Immunofluorescence analysis of brachyury T in NPMSCs

To evaluate the expression of NPMSCs marker brachyury T, NPMSCs were cultured in six-well plates at 3×10^5 cells/well. After 24 h, cells were fixed in 4% paraformaldehyde and permeabilized with 0.2% triton (Sigma) for 10 min at room temperature, and subsequently incubated with 5% goat serum (CWBIO, Beijing, China) in PBS for 30 min to blocked the nonspecific binding. Anti-Brachyury T (ab209665, Abcam, dilution 1:1000) was added and allowed to bind for 1 h at 37 °C. Alexa Fluor 488-conjugated Goat Anti-Rabbit (Proteintech Group, USA, dilution 1:200) were added for 30 min at room temperature, and then counterstained with DAPI solution (KeyGEN, Nanjing, China) to label cell nuclei and imaged using an inverted microscope (IX71; Olympus Corporation; Tokyo, Japan).

High glucose treatment and treatment with hUCMSC-CM

NPMSCs were cultured to 70–80% confluency and exposed to 35 mmol/L glucose for 72 h to induce high glucose injury. NPMSCs were randomly divided into the following three groups: (1) normal control group with normal 5.5 mmol/L glucose plus 29.5 mmol/L D-mannitol to nullify the osmotic stress caused by high concentration of solute in the culture medium is not the cause for the observed cellular stress (Ctrl); (2) high glucose group (HG) incubated with 35 mmol/L glucose for 72 h; and (3) rescue group (Res) with addition of 20% MSC-CM and 80% normal medium following high glucose treatment for 48 h. (4) normal control group with p38 MAPK inhibitor (10 µM SB203580, Sigma-Aldrich) (SB). (5) p38 MAPK inhibitor (10 µM SB203580) was added to the medium 1 h before the addition of 35 mmol/L high glucose (HG + SB).

Apoptosis and cell cycle stage detection by flow cytometry

Apoptosis was examined by flow cytometry with annexin V/propidium iodide double staining (BD Biosciences, Franklin Lakes, NJ, USA). The cell cycle stage was also evaluated by flow cytometry with propidium iodide (PI) staining (Beyotime, Shanghai, China), according to the manufacturer's instructions. The analyses were performed using fluorescence-activated cell sorting system as described above.

Real-time PCR (qPCR)

Total RNA was obtained from each group of NPMSCs using Trizol (Invitrogen, Carlsbad, CA, USA) according to the manufacturer's protocol. qRT-PCR was carried out to analyze the expression levels of ECM genes (including collagen I and II, fibronectin (FN), integrin and aggrecan). Total RNA was reverse-transcribed to cDNA using the Omniscript cDNA Synthesis Kit (Qiagen, Hamburg, Germany) according to the manufacturer's instructions and stored at − 80 °C until use. qRT-PCR was conducted using an ABI 7500 PCR system and SYBR green I dye (Toyobo, Osaka, Japan). The primers used are listed in Table 1. All reagents and primers were obtained from Bioasi Co., Ltd. (Shanghai, China). Glyceraldehyde-3-phosphate dehydrogenase (GAPDH) was used as an internal control. The expression of each gene was determined using the $2^{-\Delta\Delta CT}$ method. The qPCR conditions were as follows: 95 °C for 4 min, 94 °C for 15 s then 60 °C for 1 min, for a total of 40 cycles.

Data was analyzed using Sequence Detection Software 1.4 (Applied Biosystems, Foster City, CA, USA). Data are

Table 1 Primers for qRT-PCR

Gene name	Primer sequence		Product length (bp)
GAPDH	F	5-CTCTGCTCCTCCTGTTCGAC	121
	R	5-GCGCCCAATACGACCAAATC	
Col-I	F	5-ATCAACCGGAGGAATTTCCGTG	126
	R	5-GAGTGGTCACTCAGCATCTCA	
Col-II	F	5-TGCATGAGGGCGCGGTA	195
	R	5-GGTCCTGGTTGCCGGACAT	
Fibronectin	F	5-ACAAGCATGTCTCTCTGCCA	160
	R	5-TCAGGAAACTCCCAGGGTGA	
Integrin	F	5-CAAACAAGCCTAACGTCCGC	183
	R	5-CCACAATTTGGCCCTGCTTG	
Aggrecan	F	5-CTTCCGCTGGTCAGATGGAC	189
	R	5-CGTTTGTAGGTGGTGGCTGT	

reported as the mean ± SD of at least three independent experiments. mRNA expression is presented as fold difference with respect to untreated control groups.

Immunocytochemical analysis of ECM

For immunocytochemical analysis, NPMSCs were cultured in six-well plates at 3×10^5 cells/well in 2 mL of culture medium. After treatment, cells were fixed in 4% paraformaldehyde for 24 h and washed using 0.01 M PBS (pH 7.2–7.4). Nonspecific binding was blocked with 5% goat serum (CWBIO, Beijing, China) in PBS for 30 min. Endogenous peroxidase was blocked with 0.3% hydrogen peroxide in absolute methanol for 30 min. Anti-aggrecan (ab3778, Abcam, dilution 1:40) or anti-collagen II (ab34712, Abcam, dilution 1:100) antibodies were added and allowed to bind for 1 h at 37 °C. Peroxidase-conjugated secondary antibodies (CWBIO, dilution 1:200) were added for 30 min at room temperature. The cells were then washed three times in PBS before incubation with DAB chromogen (CWBIO) for 10 min at room temperature, and then counterstained with haematoxylin.

Western blot analysis

Western blots were performed to analyze cellular protein levels. After treatment, cells were washed twice with ice-cold PBS before lysis in radioimmunoprecipitation assay (RIPA) buffer (50 mM Tris–HCl (pH 8.0), 150 mM NaCl, 1% Nonidet P-40, 0.5% deoxycholate and 0.1% SDS) containing protease and phosphatase inhibitors (Roche Diagnostics GmbH, Mannheim, Germany). Total protein concentration in cell lysates was determined using a Bradford assay kit (BioRad, Hercules, CA, USA) according to the manufacturer's instructions. Protein extracts (3 μg/μL) were run in a 7% SDS-polyacrylamide gel by electrophoresis and transferred onto Immobilon-P membranes (EMD, Millipore). Membranes were blocked with 5% skim milk in Tris-buffered saline–Tween 20 [20 mM Tris–HCl (pH 7.6), 137 mM NaCl and 0.1% Tween 20 (vol/vol)] at room temperature for 1 h. The membranes were next incubated with primary antibodies anti-Bcl-2 (ab32124, dilution 1:1000), Anti-Bax (ab53154, dilution 1:800), anti-p38 MAPK (total, ab32142, dilution 1:10000), Anti-p38 (phospho T180 + Y182, ab4822, dilution 1:1000), Anti-Collagen II (ab34712, dilution 1:5000), Anti-Aggrecan (ab3778, dilution 1:100), and anti-GAPDH (ab8245, dilution 1:10000) (all obtained from Abcam) in blocking buffer at 4 °C overnight. After incubation with HRP-conjugated secondary antibodies (CWBIO), immunoreactive bands were detected by an enhanced chemical luminescence (ECL, Beyotime) and quantified using C-Digit (Model:3600, Image Studio Digits Ver 4.0, Licor, Lincoln, NE).

Statistical analysis

Data was analyzed using SPSS software version 17.0 (SPSS Inc., Chicago, IL, USA). Quantitative data are described as mean ± SD. Data were compared by ANOVA or Student's *t* test. A *P* value of less than 0.05 was considered statistically significant.

Results

Characterization of hUCMSCs and hUCMSC-EXO microRNAs array analysis

The adherent cells isolated from the umbilical cord formed spindle-shaped cells (Fig. 1a) and flow cytometric analysis revealed that the cells expressed a set of MSC markers, including stromal markers (CD29, CD73, CD90, and CD105). Furthermore, they did not express CD24 and hematopoietic marker CD45 (Fig. 1d). The results of induced differentiation are listed in our published papers [19]. We used gradient ultracentrifugation to extract exosomes from the MSC-CM (Fig. 1b, c). The miRNAs array results indicated that at least 100 kinds of miRNAs existed in hUCMSCs-EXO. The top 10 miRNAs with the highst abundance and its related references were listed in Table 2. We used two databases (mirBase and TargetScan) to predict and analyze the potential target genes of these miRNAs. These results prove that these microRNAs had a relationship with oncology, inflammation, and cell proliferation, and could participate in regulation of the NPMSCs repair.

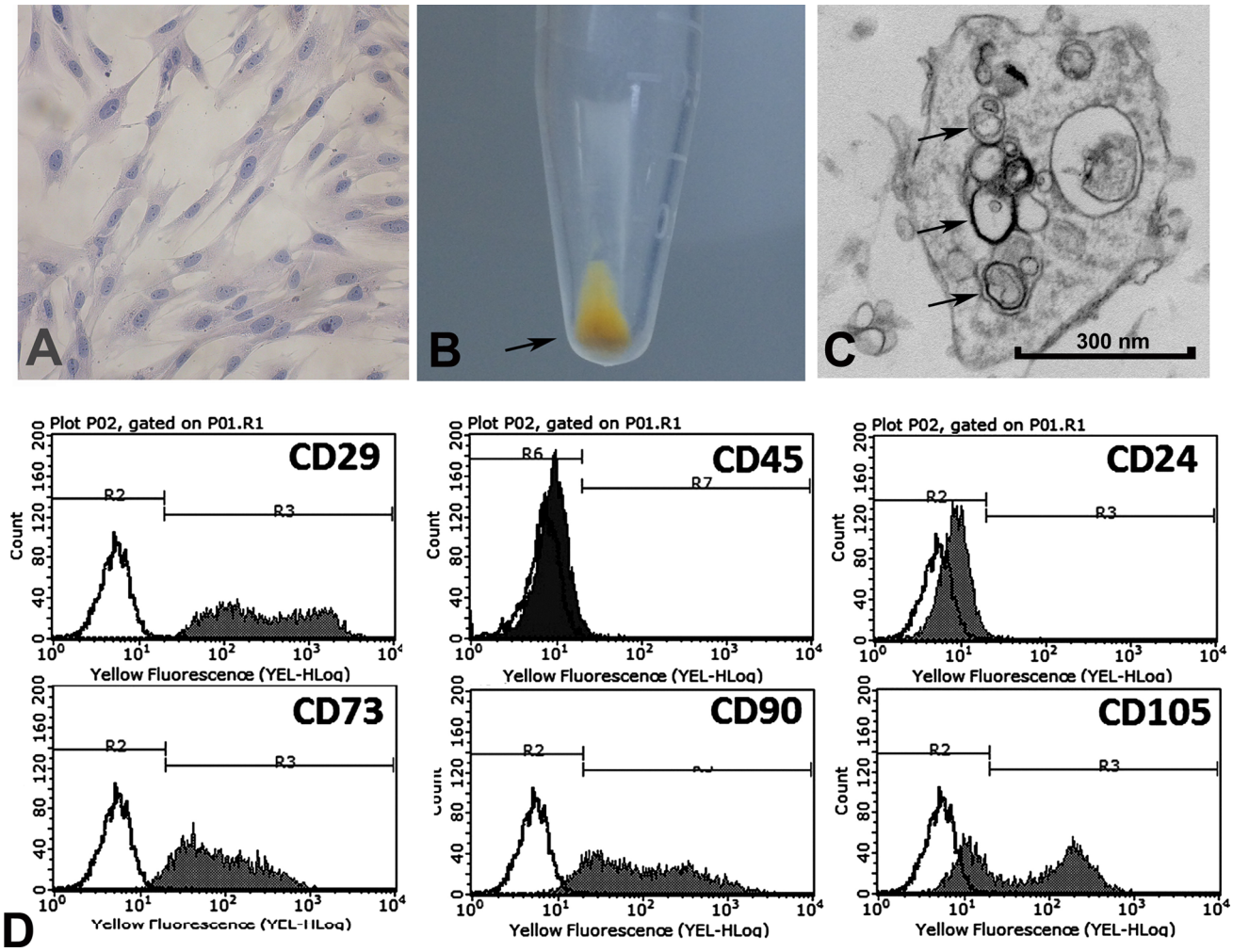

Fig. 1 Characterization of human umbilical cord mesenchymal stem cells (hUCMSCs). **a** Representative image of H&E staining of hUCMSCs (200× magnification); **b** The exosomes deposited at the bottom of the test tube after ultracentrifugation; **c** TEM showed the morphology of hUCMSCs derived exosomes, which were 30–200 nm in diameter, as shown by the arrowhead. **d** Flow cytometry analysis for hUCMSC surface marker expression

Biological characteristics of NPMSCs

Adherent cells from NP tissue with fibroblast morphology were observed as early as 48 h using the collagenase digestion method. The cells formed a monolayer of homogeneous bipolar spindle-like cells with a whirlpool-like array within 2 weeks. After several passages, adherent cells from the NP could form a monolayer of typical fibroblastic cells (Fig. 2a–d). These cells expressed CD24, CD73, CD90, and CD105. But they did not express CD29 and CD45 (Fig. 2e). In addition, Brachyury T was also detected in the nucleus region of these NP cells (Fig. 2f).

Protective effect of hMSC-CM on apoptosis and cell cycle of NPMSCs exposed to high glucose

According to annexin V/PI flow cytometry analysis (Fig. 3a, b), HG leads to an increase in the rate of NPMSCs apoptosis. The percent of cell apoptosis in the control, HG and hMSC-CM treated group was $10.99\% \pm 0.58\%$, $21.6\% \pm 1.84\%$, and $12.87\% \pm 0.62\%$, respectively. Living cells were $84.37\% \pm 2.83\%$, $65.95\% \pm 3.25\%$, and $79.70\% \pm 4.04\%$, respectively. Compared with the HG group, cells treated with hMSC-CM had a reduction in HG induced apoptosis and an increased proportion of living cells ($P<0.05$). As

Table 2 The microRNAs derived from hUC-MSCs-EXO ($n=3$)

MicroRNAs	ΔCt (mean ± SD)	Some target genes predict[a]	Published reference
miR-221-3p/222-3p	21.50 ± 2.41	Cyclin-dependent kinase inhibitor 1B (**CDKN1B**); gamma-aminobutyric acid (**GABA**); A receptor, alpha 1 (**GABRA1**) eukaryotic translation initiation factor 5A2 (**EIF5A2**)	Breast cancer [41]; Cartilage degradation [42]; Acute myocardial infarction [43]
miR-574-3p	22.47 ± 2.15	Clarin 3(**CLRN3**); serpin peptidase inhibitor (**SERPINI2**); solute carrier family 6 (**SLC6A3**)	Osteosarcoma [44]; Vascular repair [45]
let-7a-5p	22.66 ± 2.27	High mobility group AT-hook 2 (HMGA2); AT rich interactive domain 3B (**ADID3B**)	Colorectal carcinoma [46]; Cell proliferation [47]
miR-23a-3p	22.66 ± 2.62	Peptidylprolyl isomerase F (**PPIF**); plakophilin 4 (**PKP4**)	Insulin resistance [48]; Pancreatic β-Cells [49]
miR-146a-5p	24.46 ± 1.85	Immunoglobulin superfamily, member 1(**IGSF1**); interleukin-1 receptor-associated kinase 1 (**IRAK1**); TNF receptor-associated factor 6 (**TRAF6**)	Oesophageal squamous cell carcinoma [50]; Angiogenesis [51]
miR-320a	24.99 ± 1.73	TP53 regulated inhibitor of apoptosis 1 (**TRIAP1**); nucleic acid binding protein 1 (**NABP1**)	Chondrocyte degradation [52]; Ovarian development [53]; Cell proliferation and migration [54]
miR-193b-3p	25.16 ± 1.96	Interleukin 17 receptor D (**IL17RD**); Fli-1 proto-oncogene (**FLI1**); solute carrier family 39 member 5 (**SLC39A5**)	Transforming growth factor-β signaling [55]; Radio-resistance [56]
miR-125a-5p	25.28 ± 2.84	DNA-damage regulated autophagy modulator 2 (**DRAM2**); glucosaminyl (N-acetyl) transferase 1, core 2 (**GCNT1**)	Cell migration [57]; Lung tumorigenesis [58]
miR-21-5p	25.39 ± 1.75	Zinc finger protein 367 (**ZNF367**); interleukin 12A (**IL12A**); Fas ligand (**FASLG**)	Type 1 Diabetes [59]; Macrophages [60].
UniSp6 (U6)	23.3 ± 2.11	N/A	N/A

[a]We used two algorithms, namely miRBase (http://www.mirbase.org/), and TargetScan (http://www.targetscan.org/) to predict the corresponding downstream target genes of the miRNAs

shown in Fig. 3c, d, HG injury also resulted in a markedly decrease in the percentage of cell population in the G0/G1 phase and a slight, but not significant increase of cells in the S and G2/M phase, suggesting that HG induces cell cycle arrest of NPMSCs at the G1/S transition. This effect of HG was abolished with hMSC-CM treatment ($P<0.05$). Our study also demonstrates that hMSC-CM could protect NPMSCs from injury by modulating apoptosis and mitosis by increasing Bcl-2 expression and reducing Bax expression. SB203580, an inhibitor of p38 MAPK, has a similar effect (Fig. 4).

Influence of HG on ECM mRNA expression

We also investigated the effect of HG on the expression of ECM mRNA expression in cultured NPMSCs. After HG treatment for 72 h, we performed qPCR assays. Treatment with HG significantly inhibited collagen II and aggrecan mRNA expression in NPMSCs ($P<0.05$, Fig. 5a). Notably, HG exerted no marked effect on the expression of collagen I, FN and integrin mRNA.

Based on the qPCR data, the expression of collagen II and aggrecan was examined by immunocytochemistry and western blot. NPMSCs in the HG group maintained their morphology compared with the control group. However, HG reduced collagen II and aggrecan protein expression. After hMSCs-CM treatment, the expression of these two ECM components was restored ($P<0.05$, Fig. 5b–d).

MAPK activation and effect of p38 MAPK inhibitor

Exposure to a high concentration of glucose resulted in phosphorylation of p38 MAPK, without altering total p38 MAPK expression. When treated with hMSCs-CM, phosphorylated p38 MAPK levels of NPMSCs were significantly reduced but did not return to control levels (Fig. 6). SB203580, an inhibitor of p38 MAPK, alleviated HG-induced phosphorylation of p38 (Fig. 6). The addition of SB20358 restored the expression of collagen II and aggrecan on NPMSCs in HG group (Fig. 5b–d). SB203580 also relieved HG induced apoptosis (Fig. 3a, b) and cell cycle arrest in NPMSCs (Fig. 3c, d).

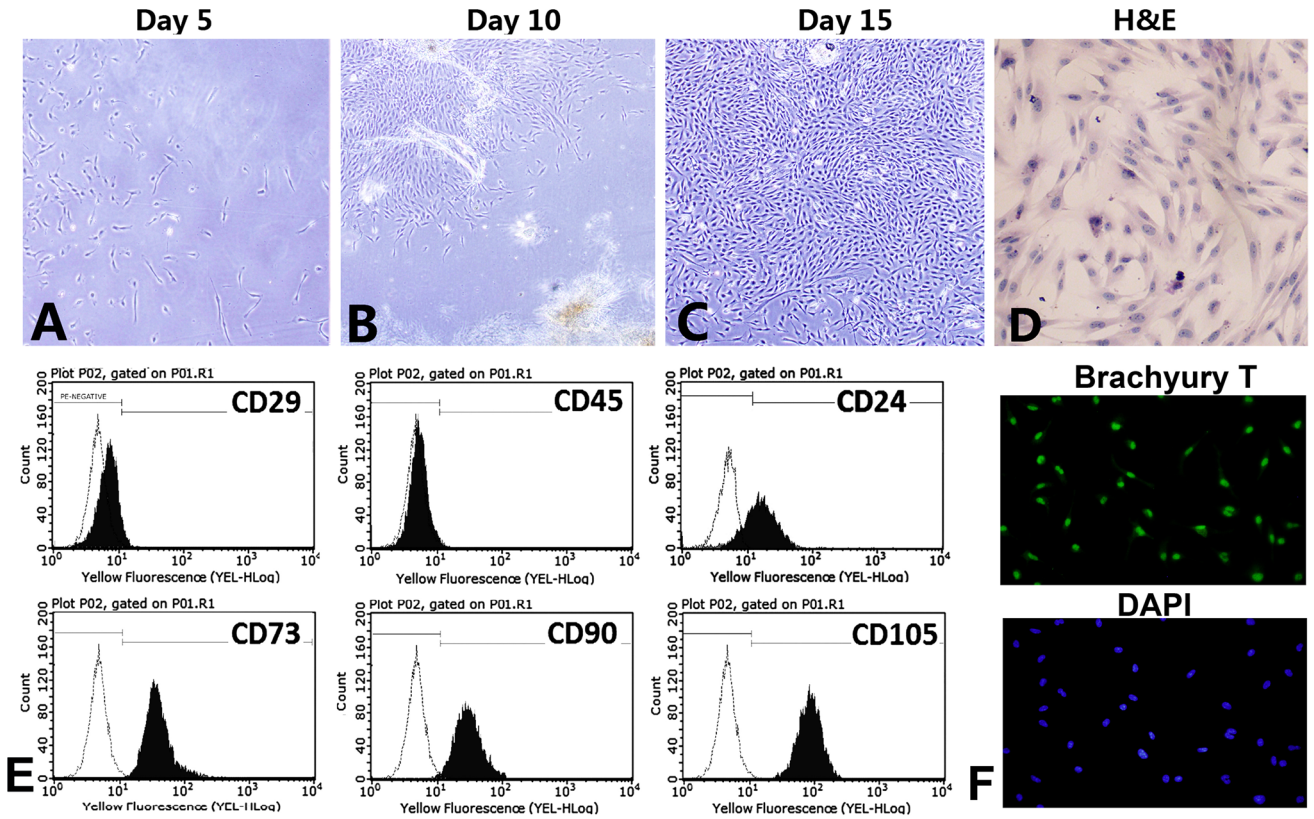

Fig. 2 Characterization of nucleus pulposus mesenchymal stem cells. **a**–**c** Representative images of NPMSCs at different stages of growth (all 100 × magnification). **d** Representative H&E staining of NPMSCs (200 × magnification). **e** Flow cytometry analysis for NPMSCs surface marker expression. **f** Immunofluorescence analysis of NPMSCs marker brachyury T. The green fluorescence signal represents the expression of brachyury T, and the blue fluorescence is DAPI stained the nucleus location (200 × magnification)

Discussion

In this study, we successfully isolated, cultured and expanded NPMSCs from the intervertebral disc using an enzymolysis method. NPMSCs were demonstrated to express collagen II and aggrecan proteins. hUCMSCs could be induced into osteoblasts and adipocytes under suitable conditions. We obtained NPMSCs and UCMSCs in line with other literature reports to determine the effects of HG concentrations on cell viability [20, 21]. Annexin V/PI double staining showed that the there was significantly more NPMSCs undergoing apoptosis in HG conditions.

Diabetes mellitus is considered to be an important etiologic factor for IDD, resulting in degenerative disc diseases. HG conditions are known to accelerate autophagy in NPMSCs [22]. Diabetes results in accumulation of AGEs in the spine and associated spinal pathology via increased catabolism. AGEs increase reactive-oxygen-species (ROS) and inflammation, and are one of the causes for the early development of diabetes mellitus [21]. It is known that ROS mediated mitochondrial dysfunction plays a critical role in HG-induced NPMSCs injury and negatively regulates the expression of type II collagen and aggrecan [23]. The accumulation of AGEs and their interaction with their receptor in the NP might result in the down-regulation of aggrecan leading to disc degeneration [21]. Our experimental results showed that the NPMSCs treated with HG increased not only apoptosis, but also increased the number of cells stuck in the S and G2/M phases. The expression of collagen II and aggrecan decreased significantly in NPMSCs as well.

Our study demonstrates that MSC-CM could protect NPMSCs from HG injury by adjusting apoptosis and mitosis by increasing Bcl-2 expression and reducing Bax expression. The Bcl-2 family of proteins includes the anti-apoptotic protein, Bcl-2, and pro-apoptotic protein, Bax. These two proteins are usually considered as biomarkers for the intrinsic pathway [24]. Bax promotes caspase activity; however, Bcl-2 is considered to be involved in caspase inhibition and thus in inhibition of apoptosis. Therefore, the Bcl-2: Bax ratio may be used to estimate cell sensitivity to apoptosis [25]. hUCMSCs are one of a few stem cell types to be applied in clinical practice as therapeutic agents for immunomodulation and ischemic tissue repair [26]. In addition to their multi-potent differentiation potential, a strong paracrine

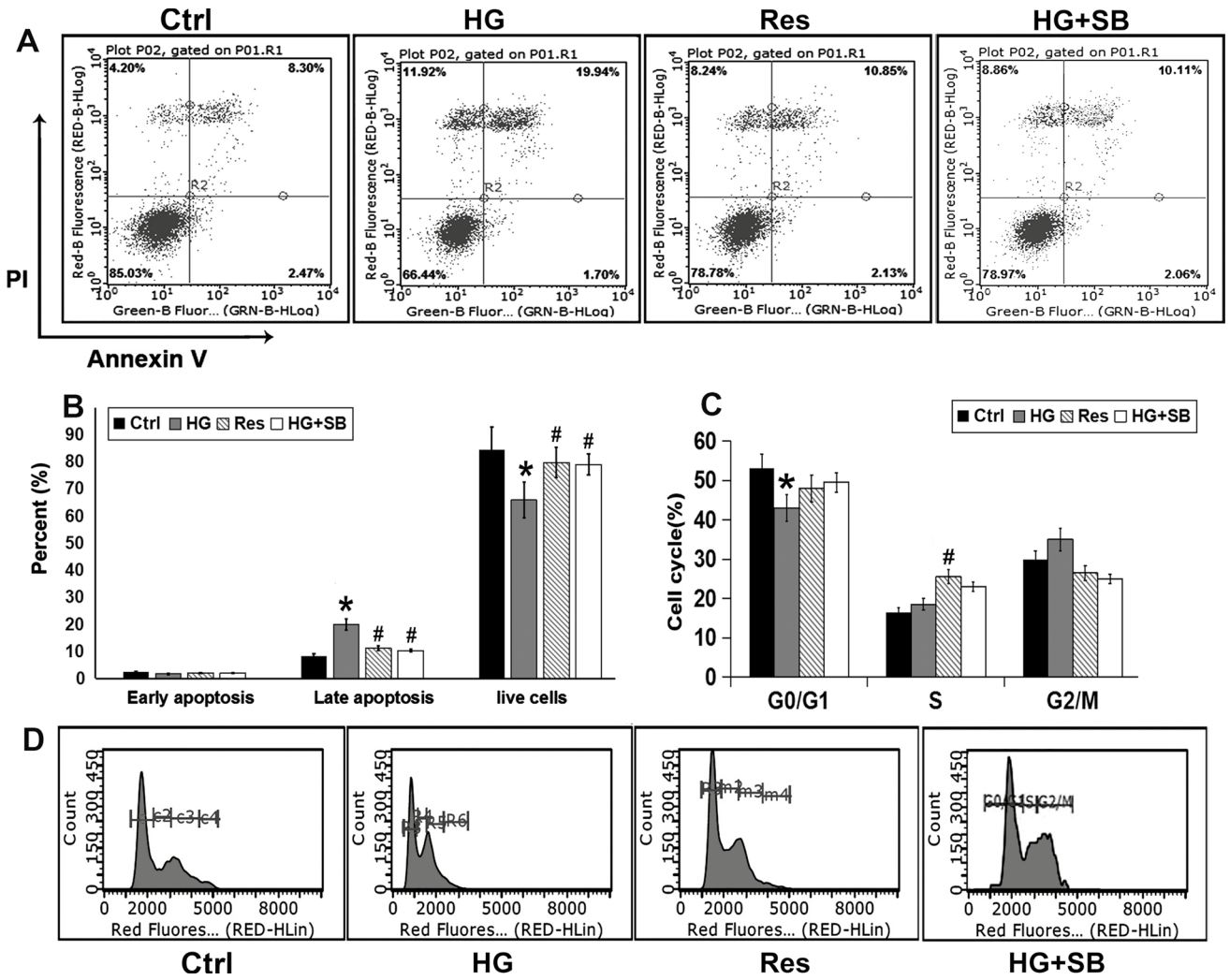

Fig. 3 Mesenchymal stem cell conditioned medium (MSC-CM) or p38 MAPK inhibitor (SB203580) treatment decreases apoptosis and regulated the cell cycle of nucleus pulposus (NP) cells. **a**, **b** Apoptosis examined by Annexin V/PI double staining flow cytometry. **c**, **d** Cell cycle distribution of NPMSCs. Data are represented as mean ± SD, $n = 9$. $^{*}P < 0.05$ vs. Ctrl group; $^{\#}P < 0.05$ vs. HG group

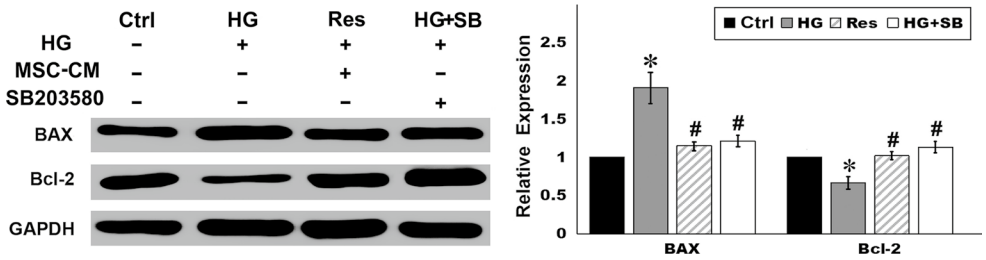

Fig. 4 Apoptosis-related protein expression by western blot in high glucose (HG) injury and mesenchymal stem cell conditioned medium (MSC-CM) treatment. MSC-CM increased Bcl-2 expression and reduced Bax expressions to protect high glucose damaged NPMSCs. MAPK p38 inhibitor (SB203580) also could increase Bcl-2 expression and reduce Bax expression. Data are represented as mean ± SD, $n = 9$. $^{*}P < 0.05$ vs. Ctrl group; $^{\#}P < 0.05$ vs. HG group

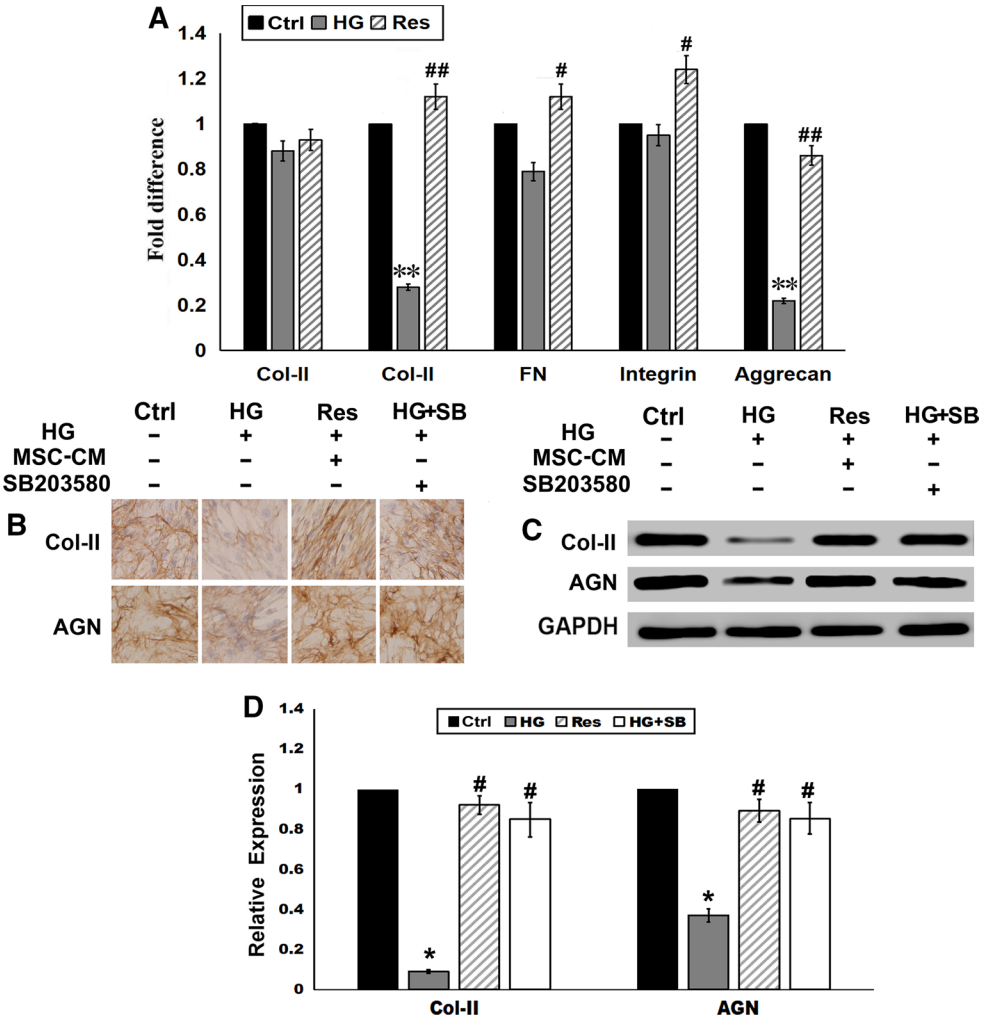

Fig. 5 Effect of high glucose (HG) and mesenchymal stem cell conditioned medium (MSC-CM) on the expression of extracellular matrix (ECM) proteins in NPMSCs. **a** mRNA expression of collagen (Col)-I, Col-II, fibronectin (FN), integrin and aggrecan is presented as the fold difference with respect to the control group. Data are represented as mean ± SD, $n = 9$; Immunohistochemical staining (**b**) and west blot analysis (**b**, **d**) of Col-II and aggrecan in NPMSCs. All images are at 200× magnification. Data are represented as mean ± SD, $n = 9$. $^{*}P < 0.05$, $^{**}P < 0.01$ vs. Ctrl group; $^{\#}P < 0.05$, $^{\#\#}P < 0.01$ vs. HG group

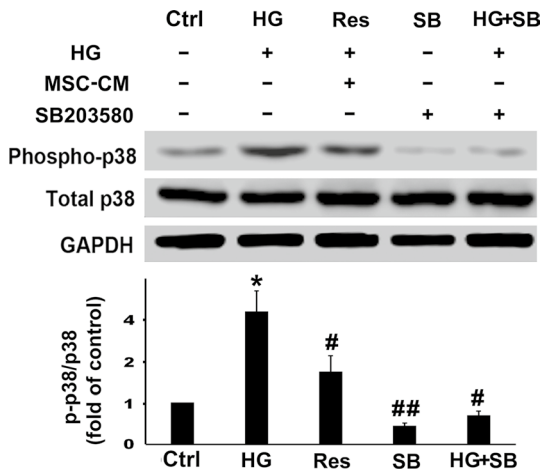

Fig. 6 Effect of HG and MSC-CM on the expression of phosphorylated p38 in NPMSCs. High glucose increased phosphorylation of p38 MAPK, whereas MSCs-CM and MAPK p38 inhibitor (SB203580) could reverse this trend. Data are represented as mean ± SD, $n = 9$. $^{*}P < 0.05$ vs. Ctrl group; $^{\#}P < 0.05$, $^{\#\#}P < 0.01$ vs. HG group

capacity has been proposed as the principal mechanism that contributes to tissue repair [26–28]. A number of cytokines were identified in MSC-CM, including vascular endothelial growth factor—A (VEGF-A), fibroblast growth factor 2 (FGF-2), hepatocyte growth factor (HGF), transforming growth factor β1 (TGF-β1), and granulocyte-colony stimulating factor (G-CSF) [27–29]. Our miRNAs array results and bioinformatics analysis predicted that miR-221-3p, let-7a-5p, and miR-21-5p derived from hUCMSCs-EXO may be closely related to extracellular matrix synthesis of NPMSCs. The trophic activity of MSCs may play a role in damage repair by affecting anti-apoptotic, proliferation, and migration pathways, along with a contribution to ECM deposition [27, 29]. Our current results indicated that the Bcl-2 expression levels in the MSC-CM treated group were notably higher than those in the HG group, while Bax expression significantly decreased.

Apart from cytokine secretion, MSCs also secrete small biological membrane vesicles known as exosomes for tissue regeneration [30]. hUCMSCs exosomes could repair CCl4 or cisplatin-induced liver damage by ameliorating

oxidative stress and cell apoptosis, inhibiting EMT and promoting cell proliferation [31, 32]. Moreover, hUC-MSC exosomes are able to improve cardiac systolic function, reduce cardiac fibrosis and protect myocardial cells from apoptosis [33]. In this study, the ability of MSC-CM to protect NPMSCs against HG induced injury may be derived from the abundant cytokines and exosomes released. MSCs are able to secrete cytokines that either antagonize the apoptotic pathway or enhance survival, such as Bcl-2, survivin, and Akt [34, 35]. The predominantly expressed Bcl-2 protein prevents the release of caspase activators; thus, cells are less likely to respond to apoptotic signaling [36]. Moreover, hUCMSCs may regulate cell growth and apoptosis by exosomal shuttle of RNA [37]. For example, three specific miRNAs (miR-21, miR-146a, and miR-181) present in hUCMSC exosomes have regulatory functions on inflammation [38].

Degradation and loss of ECM proteins (e.g., aggrecan and collagen II) are a hallmark of IDD. HG also leads to ECM degeneration in intervertebral disc tissues. AGEs were found to significantly suppress the expression of aggrecan [6, 39]. In addition, following MSCs-CM treatment, there was up-regulation of collagen II and aggrecan. Previous studies showed that inflammation could also induce ECM degradation in the NP through MAPK pathways [40]. In the present study, phosphorylated-p38 was significantly upregulated following HG treatment, whereas MSC-CM was able to reverse this trend in NPMSCs. Our data also showed that MSC-CM also up-regulated the expression of collagen II and aggrecan significantly.

In summary, this study showed that MSC-CM has potential to alleviate HG induced apoptosis and ECM degradation, and the MAPK pathways play an important role in this process. Additional studies in animal models are required to really appreciate the long-term safety and efficacy of regenerative medicine approaches in IDD.

Acknowledgements We thank Dr. Li Anna, from the Shandong maternity hospital, for providing us with flow analysis technology support.

Author contributions LQ is responsible for cytological experiments and manuscript writing. RW is responsible for molecular biology analysis. QS is responsible for immunohistochemistry. MY and MJ are responsible for west blot. LD is responsible for the overall experimental design and data analysis.

Funding This work was supported by Shandong Province Natural Science Fund (ZR2015HM053 & 2017GSF218015), the National Natural Science Foundation of China (81473484), and Shandong Province Science and Technology Research Plan (ZR2014HP053).

Compliance with ethical standards

Conflict of interest The authors declare that they have no conflict of interest.

References

1. Le Maitre CL, Freemont AJ, Hoyland JA (2005) The role of interleukin-1 in the pathogenesis of human intervertebral disc degeneration. Arthritis Res Ther 7:R732–R745
2. Chen S, Hu ZJ, Zhou ZJ, Lin XF, Zhao FD, Ma JJ, Zhang JF, Wang JY, Qin A, Fan SW (2015) Evaluation of 12 novel molecular markers for degenerated nucleus pulposus in a Chinese population. Spine (Phila Pa 1976) 40:1252–1260
3. Hammes HP, Alt A, Niwa T, Clausen JT, Bretzel RG, Brownlee M, Schleicher ED (1999) Differential accumulation of advanced glycation end products in the course of diabetic retinopathy. Diabetologia 42:728–736
4. Teillet L, Verbeke P, Gouraud S, Bakala H, Borot-Laloi C, Heudes D, Bruneval P, Corman B (2000) Food restriction prevents advanced glycation end product accumulation and retards kidney aging in lean rats. J Am Soc Nephrol 11:1488–1497
5. Boubriak OA, Watson N, Sivan SS, Stubbens N, Urban JP (2013) Factors regulating viable cell density in the intervertebral disc: blood supply in relation to disc height. J Anat 222:341–348
6. Sivan SS, Tsitron E, Wachtel E, Roughley P, Sakkee N, van der Ham F, Degroot J, Maroudas A (2006) Age-related accumulation of pentosidine in aggrecan and collagen from normal and degenerate human intervertebral discs. Biochem J 399:29–35
7. Fields AJ, Berg-Johansen B, Metz LN, Miller S, La B, Liebenberg EC, Coughlin DG, Graham JL, Stanhope KL, Havel PJ, Lotz JC (2015) Alterations in intervertebral disc composition, matrix homeostasis and biomechanical behavior in the UCD-T2DM rat model of type 2 diabetes. J Orthop Res 33:738–746
8. Luoma K, Riihimäki H, Luukkonen R, Raininko R, Viikari-Juntura E, Lamminen A (2000) Low back pain in relation to lumbar disc degeneration. Spine (Phila Pa 1976) 25:487–492
9. Jiang L, Zhang X, Zheng X, Ru A, Ni X, Wu Y, Tian N, Huang Y, Xue E, Wang X, Xu H (2013) Apoptosis, senescence, and autophagy in rat nucleus pulposus cells: implications for diabetic intervertebral disc degeneration. J Orthop Res 31:692–702
10. Hu J, Yan Q, Shi C, Tian Y, Cao P, Yuan W (2017) BMSC paracrine activity attenuates interleukin-1β-induced inflammation and apoptosis in rat AF cells via inhibiting relative NF-κB signaling and the mitochondrial pathway. Am J Transl Res 9:79–89
11. Cunha C, Almeida CR, Almeida MI, Silva AM, Molinos M, Lamas S, Pereira CL, Teixeira GQ, Monteiro AT, Santos SG, Gonçalves RM, Barbosa MA (2017) Systemic delivery of bone marrow mesenchymal stem cells for in situ intervertebral disc regeneration. Stem Cells Transl Med 6:1029–1039
12. Maidhof R, Rafiuddin A, Chowdhury F, Jacobsen T, Chahine NO (2017) Timing of mesenchymal stem cell delivery impacts the fate and therapeutic potential in intervertebral disc repair. J Orthop Res 35:32–40
13. Marfia G, Campanella R, Navone SE, Zucca I, Scotti A, Figini M, Di Vito C, Alessandri G, Riboni L, Parati E (2014) Potential use of human adipose mesenchymal stromal cells for intervertebral disc regeneration: a preliminary study on biglycan-deficient murine model of chronic disc degeneration. Arthritis Res Ther 16:457
14. Noriega DC, Ardura F, Hernández-Ramajo R, Martín-Ferrero MÁ, Sánchez-Lite I, Toribio B, Alberca M, García V, Moraleda JM, Sánchez A, García-Sancho J (2017) Intervertebral disc repair by allogeneic mesenchymal bone marrow cells: a randomized controlled trial. Transplantation 101:1945–1951
15. Liu MH, Bian BS, Cui X, Liu LT, Liu H, Huang B, Cui YH, Bian XW, Zhou Y (2016) Mesenchymal stem cells regulate mechanical properties of human degenerated nucleus pulposus cells through SDF-1/CXCR4/AKT axis. Biochim Biophys Acta 1863:1961–1968

16. Yang H, Cao C, Wu C, Yuan C, Gu Q, Shi Q, Zou J (2015) TGF-βl suppresses inflammation in cell therapy for intervertebral disc degeneration. Sci Rep 5:13254
17. Zhang B, Wang M, Gong A, Zhang X, Wu X, Zhu Y, Shi H, Wu L, Zhu W, Qian H, Xu W (2015) HucMSC-exosome mediated-wnt4 signaling is required for cutaneous wound healing. Stem Cells 33:2158–2168
18. Chen X, Zhu L, Wu G, Liang Z, Yang L, Du Z (2016) A comparison between nucleus pulposus-derived stem cell transplantation and nucleus pulposus cell transplantation for the treatment of intervertebral disc degeneration in a rabbit model. Int J Surg 28:77–82
19. Li J, Li D, Liu X, Tang S, Wei F (2012) Human umbilical cord mesenchymal stem cells reduce systemic inflammation and attenuate LPS-induced acute lung injury in rats. J Inflamm (Lond) 9:33
20. Zong S, Zeng G, Fang Y, Peng J, Zou B, Gao T, Zhao J (2016) The effects of α-zearalanol on the proliferation of bone-marrow-derived mesenchymal stem cells and their differentiation into osteoblasts. J Bone Miner Metab 34:151–160
21. Kong CG, Park JB, Kim MS, Park EY (2014) High glucose accelerates autophagy in adult rat intervertebral disc cells. Asian Spine J 8:543–548
22. Cheng X, Ni B, Zhang F, Hu Y, Zhao J (2016) High glucose-induced oxidative stress mediates apoptosis and extracellular matrix metabolic imbalances possibly via p38 MAPK activation in rat nucleus pulposus cells. J Diabetes Res 2016:3765173
23. Serban AI, Stanca L, Geicu OI, Munteanu MC, Costache M, Dinischiotu A (2015) Extracellular matrix is modulated in advanced glycation end products milieu via a RAGE receptor dependent pathway boosted by transforming growth factor-β1 RAGE. J Diabetes 7:114–124
24. Nguyen KC, Willmore WG, Tayabali AF (2013) Cadmium telluride quantum dots cause oxidative stress leading to extrinsic and intrinsic apoptosis in hepatocellular carcinoma HepG2 cells. Toxicology 306:114–123
25. Yang J, Liu X, Bhalla K, Kim CN, Ibrado AM, Cai J, Peng TI, Jones DP, Wang X (1997) Prevention of apoptosis by Bcl-2: release of cytochrome c from mitochondria blocked. Science 275:1129–1132
26. Liang X, Ding Y, Zhang Y, Tse HF, Lian Q (2013) Paracrine mechanisms of mesenchymal stem cell-based therapy: current status and perspectives. Cell Transplant 23:1045–1059
27. Walter MN, Wright KT, Fuller HR, MacNeil S, Johnson WE (2010) Mesenchymal stem cell-conditioned medium accelerates skin wound healing: an in vitro study of fibroblast and keratinocyte scratch assays. Exp Cell Res 316:1271–1281
28. Kim CH, Lee JH, Won JH, Cho MK (2011) Mesenchymal stem cells improve wound healing in vivo via early activation of matrix metalloproteinase-9 and vascular endothelial growth factor. J Korean Med Sci 26:726–733
29. Santos JM, Camões SP, Filipe E, Cipriano M, Barcia RN, Filipe M, Teixeira M, Simões S, Gaspar M, Mosqueira D, Nascimento DS, Pinto-do-Ó P, Cruz P, Cruz H, Castro M, Miranda JP (2015) Three-dimensional spheroid cell culture of umbilical cord tissue-derived mesenchymal stromal cells leads to enhanced paracrine induction of wound healing. Stem Cell Res Ther 6:90
30. Pashoutan Sarvar D, Shamsasenjan K, Akbarzadehlaleh P (2016) Mesenchymal stem cell-derived exosomes: new opportunity in cell-free therapy. Adv Pharm Bull 6:293–299
31. Li T, Yan Y, Wang B, Qian H, Zhang X, Shen L, Wang M, Zhou Y, Zhu W, Li W, Xu W (2012) Exosomes derived from human umbilical cord mesenchymal stem cells alleviate liver fibrosis. Stem Cells Dev 22:845–854
32. Zhou Y, Xu H, Xu W, Wang B, Wu H, Tao Y, Zhang B, Wang M, Mao F, Yan Y, Gao S, Gu H, Zhu W, Qian H (2013) Exosomes released by human umbilical cord mesenchymal stem cells protect against cisplatin-induced renal oxidative stress and apoptosis in vivo and in vitro. Stem Cell Res Ther 4:34
33. Zhao Y, Sun X, Cao W, Ma J, Sun L, Qian H, Zhu W, Xu W (2015) Exosomes derived from human umbilical cord mesenchymal stem cells relieve acute myocardial ischemic injury. Stem Cells Int 2015:761643
34. Okazaki T, Magaki T, Takeda M, Kajiwara Y, Hanaya R, Sugiyama K, Arita K, Nishimura M, Kato Y, Kurisu K (2008) Intravenous administration of bone marrow stromal cells increases survivin and Bcl-2 protein expression and improves sensorimotor function following ischemia in rats. Neurosci Lett 430:109–114
35. Wang SP, Wang ZH, Peng DY, Li SM, Wang H, Wang XH (2012) Therapeutic effect of mesenchymal stem cells in rats with intracerebral hemorrhage: reduced apoptosis and enhanced neuroprotection. Mol Med Rep 6:848–854
36. Green DR, Reed JC (1998) Mitochondria and apoptosis. Science 281:1309–1312
37. Zhang B, Shen L, Shi H, Pan Z, Wu L, Yan Y, Zhang X, Mao F, Qian H, Xu W (2016) Exosomes from human umbilical cord mesenchymal stem cells: identification, purification, and biological characteristics. Stem Cells Int 2016:1929536
38. Ti D, Hao H, Fu X, Han W (2016) Mesenchymal stem cells-derived exosomal microRNAs contribute to wound inflammation. Sci China Life Sci 59:1305–1312
39. Tsai TT, Ho NY, Lin YT, Lai PL, Fu TS, Niu CC, Chen LH, Chen WJ, Pang JH (2014) Advanced glycation end products in degenerative nucleus pulposus with diabetes. J Orthop Res 32:238–244
40. Cai F, Zhu L, Wang F, Shi R, Xie XH, Hong X, Wang XH, Wu XT (2017) The paracrine effect of degenerated disc cells on healthy human nucleus pulposus cells is mediated by MAPK and NF-κB pathways and can be reduced by TGF-β1. DNA Cell Biol 36:143–158
41. Abak A, Amini S, Estiar MA, Montazeri V, Sakhinia E, Abhari A (2018) Analysis of miRNA-221 expression level in tumors and marginal biopsies from patients with breast cancer (cross-sectional observational study). Clin Lab 64:169–175
42. Zheng X, Zhao FC, Pang Y, Li DY, Yao SC, Sun SS, Guo KJ (2017) Downregulation of miR-221-3p contributes to IL-1β-induced cartilage degradation by directly targeting the SDF1/CXCR4 signaling pathway. J Mol Med (Berl) 95:615–627
43. Coskunpinar E, Cakmak HA, Kalkan AK, Tiryakioglu NO, Erturk M, Ongen Z (2016) Circulating miR-221-3p as a novel marker for early prediction of acute myocardial infarction. Gene 591:90–96
44. Xu H, Liu X, Zhou J, Chen X, Zhao J (2016) miR-574-3p acts as a tumor promoter in osteosarcoma by targeting SMAD4 signaling pathway. Oncol Lett 12:5247–5253
45. Yao P, Wu J, Lindner D, Fox PL (2017) Interplay between miR-574-3p and hnRNP L regulates VEGFA mRNA translation and tumorigenesis. Nucleic Acids Res 45:7950–7964
46. Ghanbari R, Mosakhani N, Sarhadi VK, Armengol G, Nouraee N, Mohammadkhani A, Khorrami S, Arefian E, Paryan M, Malekzadeh R, Knuutila S (2016) Simultaneous underexpression of let-7a-5p and let-7f-5p microRNAs in plasma and stool samples from early stage colorectal carcinoma. Biomark Cancer 7:39–48
47. Fasihi-Ramandi M, Moridnia A, Najafi A, Sharifi M (2018) Inducing apoptosis and decreasing cell proliferation in human acute promyelocytic leukemia through regulation expression of CASP3 by let-7a-5p blockage. Indian J Hematol Blood Transfus 34:70–77
48. Lozano-Bartolomé J, Llauradó G, Otin MP, Altuna-Coy A, Rojo-Martínez G, Vendrell J, Jorba R, Rodríguez-Gallego E, Chacón MR (2018) Altered expression of miR-181a-5p and miR-23a-3p is associated with obesity and TNFα-induced insulin resistance. J Clin Endocrinol Metab 103:1447
49. Grieco FA, Sebastiani G, Juan-Mateu J, Villate O, Marroqui L, Ladrière L, Tugay K, Regazzi R, Bugliani M, Marchetti P, Dotta F, Eizirik D (2017) MicroRNAs miR-23a-3p, miR-23b-3p, and

miR-149-5p regulate the expression of proapoptotic BH3-only proteins DP5 and PUMA in human pancreatic β-Cells. Diabetes 66:100–112
50. Wang C, Zhang W, Zhang L, Chen X, Liu F, Zhang J, Guan S, Sun Y, Chen P, Wang D, Un Nesa E, Cheng Y, Yousef GM (2018) miR-146a-5p mediates epithelial-mesenchymal transition of oesophageal squamous cell carcinoma via targeting Notch2. Br J Cancer 118:e12
51. Simanovich E, Brod V, Rahat MM, Rahat MA (2018) Function of miR-146a-5p in tumor cells as a regulatory switch between cell death and angiogenesis: macrophage therapy revisited. Front Immunol 8:1931
52. Jin Y, Chen X, Gao ZY, Liu K, Hou Y, Zheng J (2017) The role of miR-320a and IL-1β in human chondrocyte degradation. Bone Joint Res 6:196–203
53. Sun YX, Zhang YX, Zhang D, Xu CM, Chen SC, Zhang JY, Ruan YC, Chen F, Zhang RJ, Qian YQ, Liu YF, Jin LY, Yu TT, Xu HY, Luo YQ, Liu XM, Sun F, Sheng JZ, Huang HF (2017) XCI-escaping gene KDM5C contributes to ovarian development via downregulating miR-320a. Hum Genet 136:227–239
54. Yu J, Wang L, Yang H, Ding D, Zhang L, Wang J, Chen Q, Zou Q, Jin Y, Liu X (2016) Rab14 suppression mediated by miR-320a inhibits cell proliferation, migration and invasion in breast cancer. J Cancer 7:2317–2326
55. Zhou X, Li Q, Xu J, Zhang X, Zhang H, Xiang Y, Fang C, Wang T, Xia S, Zhang Q, Xing Q, He L, Wang L, Xu M, Zhao X (2016) The aberrantly expressed miR-193b-3p contributes to preeclampsia through regulating transforming growth factor-β signaling. Sci Rep 6:19910
56. Lee ES, Won YJ, Kim BC, Park D, Bae JH, Park SJ, Noh SJ, Kang YR, Choi SH, Yoon JH, Heo K, Yang K, Son TG (2016) Low-dose irradiation promotes Rad51 expression by down-regulating miR-193b-3p in hepatocytes. Sci Rep 6:25723
57. Martínez-Acuña N, González-Torres A, Tapia-Vieyra JV, Alvarez-Salas LM (2017) MARK1 is a novel target for miR-125a-5p: implications for cell migration in cervical tumor cells. Microrna 7:54–61
58. Naidu S, Shi L, Magee P, Middleton JD, Laganá A, Sahoo S, Leong HS, Galvin M, Frese K, Dive C, Guzzardo V, Fassan M, Garofalo M (2017) PDGFR-modulated miR-23b cluster and miR-125a-5p suppress lung tumorigenesis by targeting multiple components of KRAS and NF-kB pathways. Sci Rep 7:15441
59. Lakhter AJ, Pratt RE, Moore RE, Doucette KK, Maier BF, DiMeglio LA, Sims EK (2018) Beta cell extracellular vesicle miR-21-5p cargo is increased in response to inflammatory cytokines and serves as a biomarker of type 1 diabetes. Diabetologia 61:1124–1134
60. Cui B, Liu W, Wang X, Chen Y, Du Q, Zhao X, Zhang H, Liu SL, Tong D, Huang Y (2017) Brucella omp25 upregulates miR-155, miR-21-5p, and miR-23b to inhibit interleukin-12 production via modulation of programmed death-1 signaling in human monocyte/macrophages. Front Immunol 8:708